Journal of Alloys and Compounds 509 (2011) 7389–7394

Contents lists available at ScienceDirect

Journal of Alloys and Compounds

journal homepage: www.elsevier.com/locate/jallcom

Dry mechanosynthesis of nanocrystalline calcium deficient hydroxyapatite: Structural characterisation

Carolina Mochales[a,*], Rory M. Wilson[b], Stephanie E.P. Dowker[c], Maria-Pau Ginebra[a]

[a] Biomaterials, Biomechanics and Tissue Engineering Group, Dept. Materials Science and Metallurgical Engineering, Technical University of Catalonia, Av. Diagonal 647, 08028 Barcelona, Spain
[b] School of Engineering and Materials Science, Queen Mary College University of London, Mile end Road, London E1 4NS, UK
[c] Queen Mary University of London, Barts & The London School of Medicine and Dentistry, Institute of Dentistry, Turner Street, London E1 2AD, UK

ARTICLE INFO

Article history:
Received 7 February 2011
Received in revised form 1 April 2011
Accepted 5 April 2011
Available online 21 April 2011

Keywords:
Ceramics
Mechanochemical processing
Crystal structure
Optical spectroscopy
X-ray diffraction

ABSTRACT

Dry mechanosynthesis is an efficient technique to synthesise nanocrystalline calcium deficient hydroxyapatites (CDHA). The mechanisms underlying a mechanochemical reaction are different from those triggering a dissolution mediated process, and this can have an effect on the structural features of the product. In this work, a nanocrystalline CDHA with Ca/P molar ratio of 1.5 obtained by means of dry mechanosynthesis of calcium oxide and dicalcium phosphate dihydrate was analysed. Spectroscopic techniques confirmed the presence of hydrogen phosphate (HPO_4^{2-}) groups and a non-apatitic environment of the phosphate ions and disordered hydroxyl groups due to the nanometric size of the crystals. Lattice parameters of mechanosynthesised CDHA showed a small increase in the ***a*** lattice parameter (9.4418(20) Å) and a small decrease in the ***c*** lattice parameter (6.8745(17) Å), in agreement with the values reported in the literature for precipitated CDHAs. A prolonged milling resulted in an increase of the crystallinity of the CDHA and its partial decomposition into β-TCP by the loss of OH^- and HPO_4^{2-} groups.

1. Introduction

It is nowadays well established that the mineral phase of bone is a calcium hydroxyapatite with multiple ionic substitutions, with crystals in the nanometric range (~20 nm × 40 nm × 5 nm) [1,2]. Moreover, there is increasing evidence that the replication of both the chemistry and dimensions of the bone mineral is a good strategy, which enhances the performance of bone regeneration biomaterials [3–6]. In this context, the interest in new synthesis routes for calcium deficient hydroxyapatites (CDHAs) with nanometric crystal sizes (i.e. nanocrystalline HAs) has increased during the last years.

Several synthesis methods of nanocrystalline CDHAs have been reported in the literature [7], most of them based on dissolution/precipitation mechanisms. Among them we find hydrothermal methods [8–10], sol–gel crystallization methods [11] or hydrolysis of other calcium phosphates [12,13]. A different approach which has also proven to be successful is the one based on the dry mechanochemical processing, where a solid phase reaction is achieved by mechanical activation of mixtures, involving the dispersion of solids and their plastic deformation [14]. Nanosized HA particles have been successfully obtained by milling calcium oxide (CaO) and either anhydrous dicalcium phosphate (DCP, $CaHPO_4$) [15,16] or dicalcium phosphate dihydrate (DCPD, $CaHPO_4{\cdot}2H_2O$) [16–18]. Moreover, it has been shown that this technique allows good control of the Ca/P molar ratio of the HA powders obtained, being able to synthesise calcium deficient hydroxyapatites (CDHAs) in an effective and reproducible manner [16–19]. This technique has been proved also to be effective for the synthesis of apatites with different ionic substitutions, which is also of interest to improve their biological response [20–24]. This should be of interest to those engaged in industrial scale synthesis of such materials.

Mechanosynthesis is based on the action of the impact force produced by the collision of two balls or one ball with the mill walls in the powder trapped between them. The powder experiences intense mechanical deformation and local temperature increase. This deformation and temperature increase leads to generation of crystal defects and this, plus the balance between the coalescence and fracturing events among the powder particles, is expected to trigger structural changes in the powder [14]. Thus, the mechanisms activating the chemical reaction in a mechanosynthesis process are different from the ones taking place in a solution-mediated process. It is the aim of this work to see if this can result in

* Corresponding author at: Dental Materials Science and Biomaterials Research Group Institute for Dental, Oral and Maxilary Medicine CC3 "Charité" Universitaetsmedizin Berlin Assmannshauser Str. 4-6 14197 Berlin, Germany.
E-mail address: carolina.mochales-palau@charite.de (C. Mochales).

0925-8388/$ – see front matter © 2011 Elsevier B.V. All rights reserved.
doi:10.1016/j.jallcom.2011.04.033

different structural features in the nanocrystalline CDHAs obtained by dry mechanosynthesis compared to CDHAs obtained by other routes. This study presents a detailed structural characterisation of a nanocrystalline CDHA with a theoretical Ca/P ratio of 1.5, obtained by dry mechanosynthesis, according to the following reaction:

$$6CaHPO_4{\cdot}2H_2O + 3CaO \rightarrow Ca_9(HPO_4)(PO_4)_5OH + 14H_2O \quad (1)$$

2. Materials and methods

2.1. Sample preparation

Chemicals used in CDHA mechanosynthesis were analytical reagent grade calcium oxide and dicalcium phosphate dihydrate purchased from Aldrich (CaO) and Fluka ($CaHPO_4{\cdot}2H_2O$, DCPD). DCPD and CaO were chosen as reactants because they are the phosphate and calcium salts that react faster in a mechanochemical reaction [19].

Mechanosynthesis reactions with a total mass of reactants of 40 g and a Ca/P molar ratio of 1.5, according to Eq. (1) were performed in a Pulverissette 6 planetary Fristch mill at a disc rotation speed of 350 rpm with agate vial and balls. Instrumental details of the mill, vial and balls are shown in Table 1.

2.2. Phase evolution with milling time by X-ray diffraction

Around 100–150 mg of powder were extracted at different milling times and were analysed by X-ray diffraction (XRD). A 1500 W sealed tube with a Cu target (25 mA and 40 kV) was used with a Ge 1 1 1 monochromator to give CuKα1 radiation (λ = 1.5406 Å). Diffraction patterns were collected with an INEL CPS-120 curved position sensitive detector that allows simultaneous data collection in 4096 bins over 0–120° in 2θ [25,26]. The sample holder was a (7 1 1) cut Si single crystal with the incoming monochromatic beam striking its surface at an angle of ~3.5° so as to minimize the background. Generally 10–20 mg samples dispersed in acetone were used. The sample holder was rotated about a fixed axis normal to its surface to increase the number of crystallites in differing orientations contributing to powder pattern, thus obtaining a better powder average. Each data set was collected for at least 833 min. Patterns were calibrated using curves produced from a mixture of Y_2O_3 and silver behenate run before and after each sample and of similar quality to the sample data set. The calibration curves were a least-squares spline fitted to the differences between the measured and calculated patterns (using a = 10.604 Å at 20 °C for Y_2O_3 and a = 58.529 Å for the silver behenate interplanar spacing) which gives 60 plus peaks in a range from 3 to 117° in 2θ.

2.3. Structural characterisation of a CDHA obtained by dry mechanosynthesis

A CDHA batch of powder was obtained by milling during 1 h 15 min without opening the mill at any stage of the reaction. According to the previous phase evolution analysis this milling time was enough to ensure reaction completion. The chemical composition of the resulting powder was analysed by ICP-OES in terms of Ca and P content. Since one of the main drawbacks of mechanosynthesis is the possible contamination of the powder due to the wear of the balls and the vial, the amount of agate (~SiO_2) was evaluated also by the quantification of silicon by ICP-OES. This batch of powder was used to perform a detailed structural analysis by means of spectroscopic, and diffraction techniques.

The specific surface area of the powder was measured by N_2 adsorption following the BET theory (Micromeritics, ASAP 2020).

The morphology of the mechanosynthesized CDHA was assessed by Transmission Electron Microscopy (TEM, JEOL 1200 EX-II). The powder was ultrasonically dispersed in ethanol for ten minutes and subsequently a droplet of the suspension was placed on a carbonformvar copper grid, where it was allowed to dry

2.3.1. Spectroscopy

Fourier transform infrared (FTIR) spectra of the CDHA sample were recorded using a Perkin Elmer Spectrum GX FTIR spectrometer. A CDHA powder mass of 2 mg for the detection of weak bands and 1 mg for determination of the frequencies of the very strong ν_3PO_4 bands were dispersed in a KBr matrix (300 mg).

Magic angle spinning nuclear magnetic resonance (MAS NMR) for phosphorus (^{31}P-MAS NMR) and proton (^{1}H-MAS NMR) were also recorded. The ^{31}P spectrum was measured on a Bruker Avance-600 spectrometer at a frequency of 242.94 MHz with high power proton decoupling, a spin speed of 12,000 Hz, a sweep width of 100 kHz, a repetition rate of 5.02 s and 32 scans. The ^{1}H spectrum was measured on a Bruker MSL-300 spectrometer at a frequency of 300.13 MHz with a spin speed of 10,000 Hz, a sweep width of 125 kHz, a repetition rate of 30.0 s and 248 scans.

2.3.2. Structure refinements by Rietveld analysis

X-ray diffraction (XRD) patterns of 5 CDHA samples obtained from the same batch of milled powder were recorded.

The program GSAS was used to refine the structures. The background was modelled with function type 1 (Chebyschev polynomials of the first kind) with 8 coefficients. The instrumental profile was refined from a NIST SRM 660a LaB6 sample. The peak-shape was modelled with function type 2 using GU and GW values obtained from the instrumental profile and varying LX and LY for the apatite line profile. The L11 and L22 parameters were varied in the apatite structure refinements to better fit the 0 0 2 peaks, using as initial values 0.05. Starting atomic parameters came from the refinement in $P6_3/m$ of Holly Springs HA obtained with neutron data reported by Sudarsanan and Young [27]. Occupancies and atom positions and unit cell were allowed to vary. Following the procedure used by Wilson et al. [28] and Morgan et al. [29], the Ca1 occupancy was fixed at the stoichiometric value. The H occupancy was allowed to vary, but not its positional or displacement parameters. The results reported here are all from refinements in which the anisotropic displacement parameters were fixed to those reported for Holly Springs HA [27]. Refinements were performed in the 5 CDHA samples obtained from the same batch of powder.

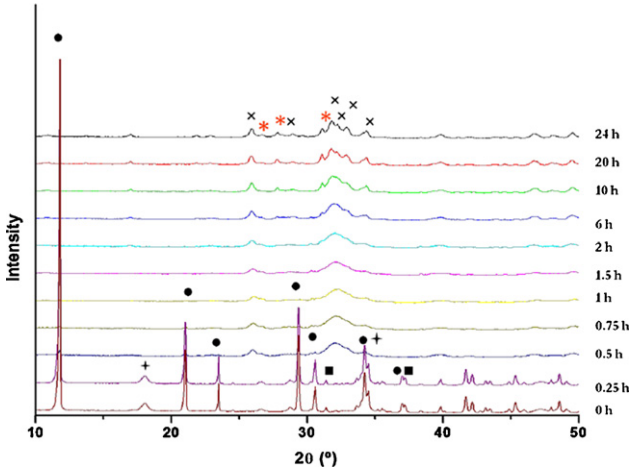

Fig. 1. XRD patterns of 40 g of a mixture of DCPD and CaO (Ca/P = 1.5) after different periods of mechanical grinding (indicated on each pattern) at 350 rpm. Main peaks: (●) DCPD, (■) CaO, (✦) ($Ca(OH)_2$, (×) HA, (✱) β-TCP.

3. Results and discussion

3.1.1. Phase evolution with milling time

Fig. 1 shows the phase evolution of the powder at different milling times. It was observed that the starting products, DCPD and $CaO/Ca(OH)_2$ (calcium hydroxide appears at short milling times due to atmospheric hydration of the samples), disappeared and an apatitic profile appeared progressively with increasing milling times as previously observed [18]. Moreover, an increase in the crystallinity of the apatitic profile with higher milling times was clearly seen. In absence of a mechanochemical reaction, it would be expected that higher milling times would lead to a reduction of crystal size, and therefore broader peaks. In contrast, in this case the crystallinity increased with milling time. After 2 h of milling, some non-apatitic peaks appeared and increased with longer milling times. These peaks were assigned to β-TCP. The formation of β-TCP may be due to the effect of the progressive milling of the already formed apatitic crystals, which fostered its partial decomposition by the loss of the HPO_4^{2-} and OH^- groups. In fact, the formation of β-TCP by mechanosynthesis is a remarkable result, since this phase is obtained only at high temperatures. It has to be taken into account, however, that during a mechanosynthesis process local increases of temperature can take place due to high energy collisions between balls or ball and wall of the mill. Nevertheless, it is not clear yet how high the temperature rise can be, and how this could influence or promote the β-TCP formation. Moreover, mechanosynthesis is a non-equilibrium process i.e. it does not operate at thermodynamic equilibrium. In order to strengthen this assignment, further investigations including IR and, or NMR spectroscopic studies after long milling times should be performed.

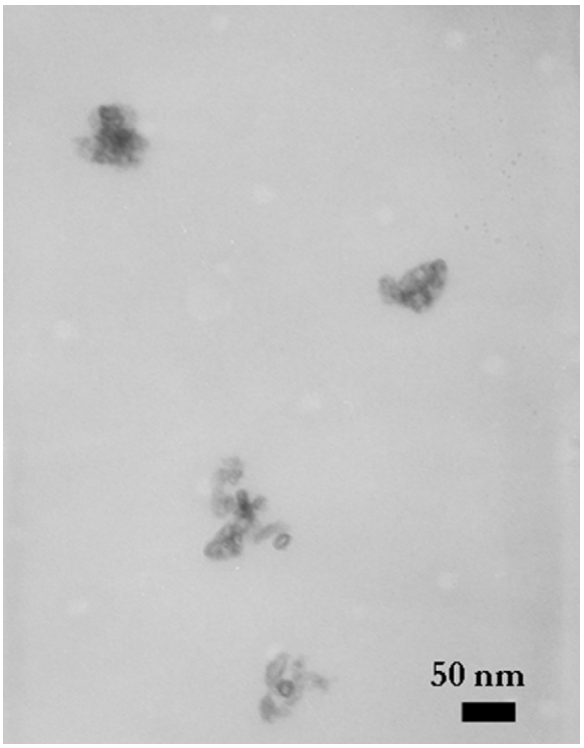

Fig. 2. TEM micrograph of the CDHA powder obtained after milling for 1 h 15 min.

According to Fig. 1 at 1 h 15 min no reactants were present and only an apatitic profile was detected. Therefore, the CDHA used for the structural analysis was milled for 1 h 15 min.

3.2. Structural characterisation

3.2.1. Chemical analysis and powder morphology

The Ca/P molar ratio obtained by ICP-OES was 1.56 ± 0.07. Moreover, the silicon content was lower than the detection limit of 0.2 wt%.

The morphology and size of the mechanosynthesised powder are shown in Fig. 2. The powder consisted of aggregates of nano-crystallites of 20–50 nm. The SSA of the powder was 113.3 ± 0.5 m^2/g.

3.2.2. Infrared spectroscopy

The FTIR spectrum of the mechanosynthesised CDHA is shown in Fig. 3. Phosphate bands were detected at 1090 and 1044 cm^{-1} (ν_3), 962 cm^{-1} (ν_1), 603 and 566 cm^{-1} (ν_4) and 472 cm^{-1} (ν_2). Hydroxyl bands characteristic of hydroxyapatite were observed at 3568 cm^{-1} (stretching) and 631 cm^{-1} (libration). Broad bands due to water were observed in the region 2500–3700 cm^{-1} and at about 1640 cm^{-1} [30].

The fairly broad absorption at 877 cm^{-1} is assigned to HPO_4^{2-}. In fact, it cannot be due to a CO_3^{2-} ν_2 mode because there is essentially no trace of any absorption in the region 1545–1410 cm^{-1} where

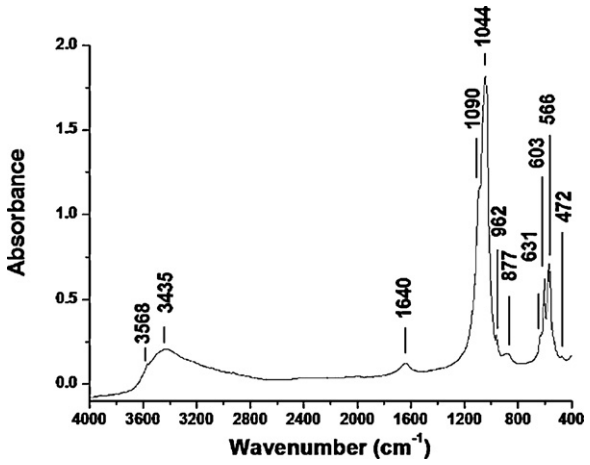

Fig. 3. Infrared spectrum of a mechanosynthesised CDHA with Ca/P molar ratio of 1.5.

the much stronger ν_3 bands would be seen. Detailed examination of this band profile (Fig. 4) suggests splitting, which may indicate the presence of HPO_4^{2-} in two different local environments. Indeed, there is a maximum at 875 cm^{-1} but also a broader absorption centred at about 890 cm^{-1}. Since these features are identical for both concentrations (1 and 2 mg), it suggests that they are real.

Detailed examination of the band profile (Fig. 4) suggests splitting, which may indicate the presence of HPO_4^{2-} in different local environments. Indeed, Fig. 3 shows another maximum at about 885 cm^{-1} and a broader absorption centred at about 890 cm^{-1}. Since these features are identical for both concentrations (1 and 2 mg), it suggests that they are real Moreover, also both concentrations (1 mg and 2 mg) in the range of the ν_4PO_4 vibration mode (500–700 cm^{-1}) showed one shoulder around 534 cm^{-1} (Fig. 5). This shoulder has been attributed by Rey et al. [31,32] to non-apatitic HPO_4^{2-} groups according to the proposed model of a hydrated surface layer existing in apatites with nano-dimensions. Moreover, this hydrated surface layer would contain relatively mobile ions (mainly, bivalent anions and cations: Ca^{2+}, HPO_4^{2-}, CO_3^{2-} in non-apatitic sites (probably OCP or DCPD) [7].

3.2.3. NMR spectroscopy

3.2.3.1. ^{31}P-NMR. ^{31}P-NMR showed a single band at 3.06 ppm (Fig. 6a). This band is close to typical values reported for ^{31}P-NMR of HA (2.77 ppm [30] and 2.8 ppm [33]. This result is also in agreement with NMR studies of precipitated CDHAs with a Ca/P molar ratio of 1.55, close to the one in this study, where a band at 2.84 ppm was reported by Wilson et al. [34]. Wilson et al. reported also a shoulder to this band at 0.5 ppm and assigned to the presence of HPO_4^{2-} groups. This additional band was not seen in mechanosynthesised CDHA spectrum. However, this additional band was not seen either in bone ^{31}P-NMR spectrum reported by Kaflak-Hachulska et al. [35], who only reported a single sharp band at 3.1 ppm, very close to the band seen at 3.06 ppm in mechanosynthesised CDHA spectrum, and neither in other precipitated CDHAs with Ca/P molar ratio of 1.5 and high SSA, as reported by Rodriguez Lorenzo [36].

Table 1
Specifications of the Pulverissette 6 (P6) planetary Fritsch mill and the vial and balls used in this work.

	Vial		Balls			Disc rotation velocity ω_d (rpm) range	Vial to disc rotation velocities rate ω_v/ω_d	Eccentricity r_d (cm)
	Radius r_v (cm)	Volume (ml)	Mean diameter (cm)	Mean weight (g)	Mean surface area (cm^2)			
P6 planetary Fritsch mill	5	500	3	37	28.3	100–600	1.82	6.08

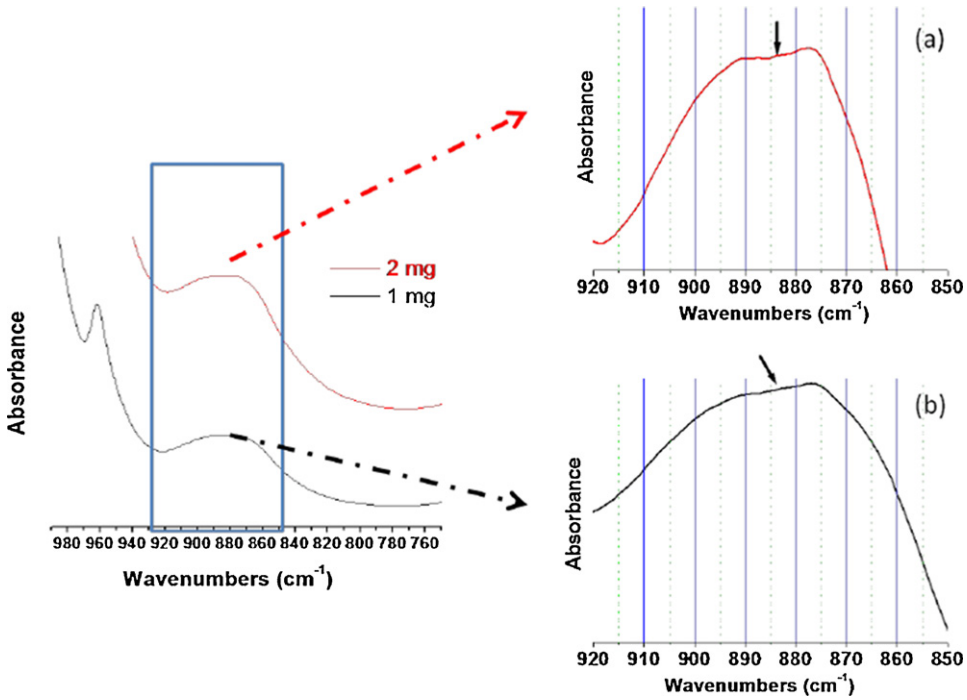

Fig. 4. Detail of 877 cm^{-1} peak from infrared spectrum showed in Fig. 2. The IR spectra obtained for both concentrations [(a) 1 mg and (b) 2 mg] were examined. The arrow shows a second peak at around 884 cm^{-1}.

3.2.3.2. ^{1}H-NMR. A broad band at 5.354 and a sharper one at −0.118 ppm were detected in the ^{1}H-NMR spectra (Fig. 6b). These bands can be attributed to water and hydroxyl groups respectively [36]. The large area of the band at 5.354 (from ~20 to −10 ppm) indicates a high water content in the samples, which could correspond to adsorbed water, enhanced by the nanometric size of the CDHA crystals. In fact, although the mechanosynthesis is performed in dry conditions, without water addition, according to Eq. (1) water is obtained as a reaction product. Previous studies showed that a CDHA with a Ca/P ratio of 1.5 obtained by this method contained around 10–15 wt% water [18].

An additional weak band around 9 ppm has been reported in some CDHA spectra and assigned to HPO_4^{2-} groups [23,32,34,36]. This weak band can be associated to the weak band observed in the mechanosynthesised CDHA spectrum around 12 ppm, although obscured by the broad water band. Looking at the CDHA spectrum in detail it is possible to see two very small bands around 1 and 2 ppm.

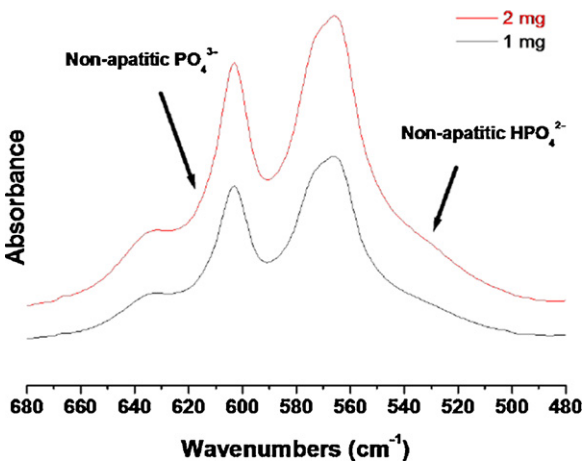

Fig. 5. Detail of the ν4PO4 vibration mode showing a shoulder around 534 cm^{-1} (arrow) attributed by Rey et al. (ref) to the non-apatitic surface layer.

These bands were first assigned to water molecules by Yesinowski and Eckert [37] in the spectra of OCP. However, the origin of these bands is unclear and different assignments have been proposed in literature. For instance, Rodríguez-Lorenzo [36] assigned a band

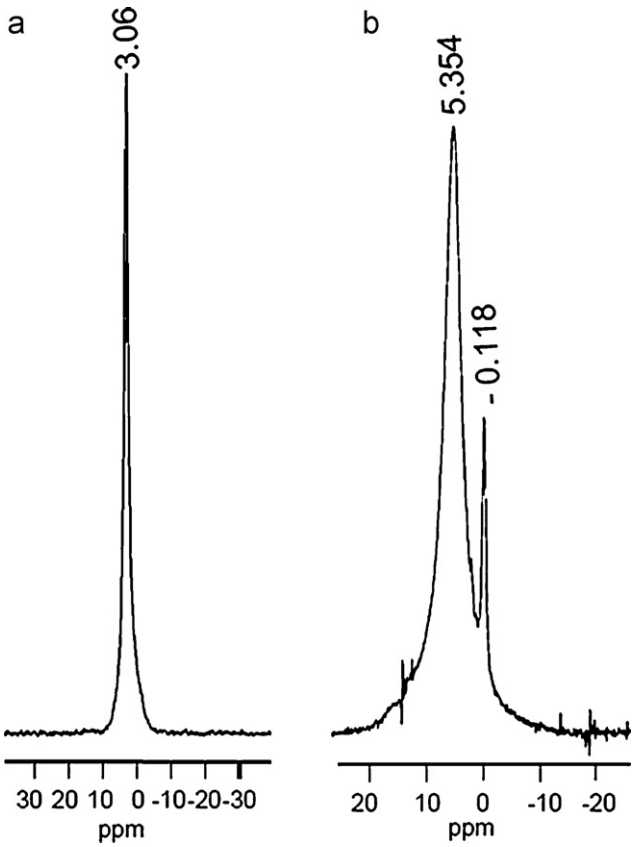

Fig. 6. NMR spectra of mechanosyntesised CDHA (Ca/P = 1.5): (a) ^{31}P-NMR and (b) ^{1}H-NMR.

Table 2
Chemical Profile *R* factors, goodness of fit χ^2, lattice parameters and cell volume of five mechanosynthesised CDHA (Ca/P = 1.5) samples obtained from the same batch of powder. Mean (standard deviation) and means for other apatites reported in the literature.

Spec	χ^2	R_{wP} (%)	R_P(%)	***a*** (Å)	***c*** (Å)	V (Å^3)
1	3.12	6.33	4.65	9.4412(4)	6.8752(3)	530.73(4)
2	5.01	6.15	4.40	9.4449(6)	6.8746(4)	531.10(5)
3	4.90	6.14	4.40	9.4421(6)	6.8762(4)	530.91(5)
4	5.23	6.29	4.53	9.4401(6)	6.8719(4)	530.34(5)
5	5.13	6.36	4.54	9.4409(6)	6.8745(4)	530.63(5)
Mean	–	–	–	9.4418(20)	6.8745(17)	530.74(29)
CDHA[a]	–	–	–	9.4320 (40)	6.8751(31)	529.68(69)[d]
HA[b]	–	3.8	–	9.4244(2)	6.8854(2)	529.62(4)[d]
HA[c]	–	–	–	9.4243(55)	6.8856(35)	529.63(89)[d]

[a] Mean and standard deviation (6 samples) reported by Wilson et al. [34].
[b] SRM 2910, calculated from results in Table 3 [29] as reported by Wilson et al. [34].
[c] Mean and Standard deviation (six samples) for high temperature HA calculated from results in penultimate row of Table 3 [29] as reported by Wilson et al. [34].
[d] Cell volumes calculated from ***a*** and ***c*** values reported in corresponding literature.

Table 3
Unit cell contents for five mechanosynthesised CDHA (Ca/P = 1.5) samples obtained from the same batch of powder (scaled so that Ca1 is 4, the stoichiometric value) with standard deviations in brackets and means for other apatites reported in the literature.

Spec.	Ca2	P	O1	O2	O3	O(H)	H	Ca/P[d]
1	6.12(2)	5.99(4)	5.77(4)	6.87(5)	11.24(10)	2.04(5)	3.30(45)	1.688
2	6.19(4)	6.06(5)	5.81(6)	6.95(7)	11.24(13)	2.17(7)	3.04(64)	1.681
3	6.09(4)	5.92(5)	5.70(5)	6.91(7)	10.88(12)	2.20(7)	2.44(65)	1.704
4	6.17(4)	6.02(5)	5.84(6)	6.94(7)	11.21(13)	2.23(7)	2.82(66)	1.689
5	6.08(4)	5.91(5)	5.73(6)	6.88(8)	10.80(13)	2.14(7)	3.14(66)	1.706
Mean	6.13(6)	5.98(8)	5.77(8)	6.91(8)	11.08(25)	2.15(10)	2.95(70)	1.694(11)
CDHA[a]	5.75(2)	5.82(4)	5.92(3)	6.28(5)	12.44(13)	2.53(7)	2.49(44)	1.675(10)
HA[b]	6.02(1)	5.86(2)	6.19(2)	6.14(2)	12.40(5)	2.22(2)	2.51(19)	1.711
HA[c]	6.11(2)	5.97(3)	6.16(2)	6.17(7)	12.59(4)	2.34(6)	2.36(64)	1.693

[a] Mean and standard deviation (6 samples) reported by Wilson et al. [34].
[b] SRM 2910, calculated from results in Table 3 [29] as reported by Wilson et al. [34].
[c] Mean and Standard deviation (6 samples) for high temperature HA calculated from results in penultimate row of Table 3 [29] as reported by Wilson et al. [34].
[d] Mole ratio calculated from Rietveld determined occupancies.

around 2 ppm in the spectra of OCP to a mobile defect; and Jäger et al. [38] proposed that bands around 1 and 2 ppm shown in nanocrystalline HA might come from structural hydroxyl groups which were possibly disordered by the presence of structural water in hydroxyl sites and thereby involved in some hydrogen bonding. This structural disorder is in good agreement with the proposed model of the existence of a fragile hydrated layer around the surface of the HA nanocrystal [7].

3.2.4. Rietveld refinement of the CDHA structure

Five samples from the same batch of powder were measured by XRD and their structures and peak shapes refined. The XRD pattern of one of these samples with its corresponding fitted refinement curve and the difference between them can be seen in Fig. 7. The refinements were begun from the structure of Holly Springs HA [27] which resulted in the structure shown in Tables 2–4.

Table 2 shows acceptable estimates of uncertainty for the 5 refinements. Compared to high temperature sintered stoichiometric HA [29] lattice parameters ***a*** and ***c*** of mechanosynthesised CDHAs have increased and decreased respectively. The expansion (from mean high temperature HA) of ***a*** is 0.0175 Å and the decrease in ***c*** is 0.0111 Å, which, results in an increase in cell volume of 1.11 Å^3. This result is very consistent with the literature. For example, in a work by Wilson et al. [34] the increase and decrease in ***a*** and ***c*** reported for a precipitated CDHA with a Ca/P ratio of 1.55 were reported as 0.0077 Å and 0.0105 Å respectively. Contrary to this result, the change in ***c*** was higher than in ***a***. However, most of the values reported in the literature [30] show a higher change in ***a*** than in ***c***, as in the CDHA mechanosynthesised here.

Unit cell contents of the CDHA refinements are shown in Table 3. It is surprising that the apparent Ca2 content is so high (6.13) and similar to high temperature HA (6.02 and 6.11), as in principle Ca2

Table 4
Positional parameters, mean (standard deviation) × 10^4 for five mechanosynthesised CDHA (Ca/P = 1.5) samples obtained from the same batch of powder and means for other apatites reported in the literature.

Spec.	Ca1*z*	Ca2*x*	Ca2*y*	*Px*	*Py*	O1*x*	O1*y*	O2*x*	O2*y*	O3*x*	O3*y*	O3*z*	O(H)*z*
1	11(5)	2386(2)	9844(3)	3947(3)	3691(3)	3402(7)	4942(8)	5720(6)	4563(6)	3417(6)	2576(6)	744(5)	1799(24)
2	3(7)	2382(3)	9851(4)	3945(4)	3692(4)	3389(9)	4950(11)	5740(8)	4576(8)	3427(8)	2577(8)	730(7)	1748(30)
3	0.1(65)	2378(3)	9843(4)	3939(4)	3693(4)	3398(9)	4930(11)	5747(8)	5747(8)	34081(8)	2575(8)	742(8)	1707(28)
4	6(6)	2381(3)	9848(4)	3946(4)	3696(4)	3394(9)	4944(11)	5740(8)	5740(8)	3420(8)	2571(8)	727(7)	1718(29)
5	5(7)	2376(3)	9840(4)	3942(5)	3698(5)	3396(9)	4930(12)	5753(8)	4596(9)	3405(8)	2571(8)	743(8)	1730(30)
Mean	5(7)	2380(5)	9845(6)	3945(5)	3694(5)	3397(10)	4941(12)	5740(14)	4582(16)	3415(11)	2574(8)	737(7)	1740(46)
CDHA[a]	29(3)	2456(1)	9920(3)	3976(2)	3686(1)	3301(5)	4881(6)	5816(5)	4621(4)	3425(4)	2595(4)	691(6)	1785(27)
HA[b]	11(2)	2464(1)	9928(1)	3979(2)	3682(1)	3280(3)	4846(3)	5854(3)	4639(3)	3415(2)	2567(2)	692(2)	1944(10)
HA[c]	11(4)	2465(1)	9926(2)	3980(2)	3676(2)	3276(5)	4850(5)	5846(4)	4629(8)	3414(4)	2559(6)	683(5)	1935(13)
Shift[d]	−6	−84	−81	−35	18	121	91	−124	−47	1	15	54	−195

[a] Mean and standard deviation (6 samples) reported by Wilson et al. [34].
[b] SRM 2910, Table 1 [29] as reported by Wilson et al. [34].
[c] Mean and Standard deviation (6 samples) for high temperature HA calculated from results in last row of Table 3 [29] as reported by Wilson et al. [34].
[d] Shift expressed as mean of the five CDHA refinements minus mean of high temperature HA [29].

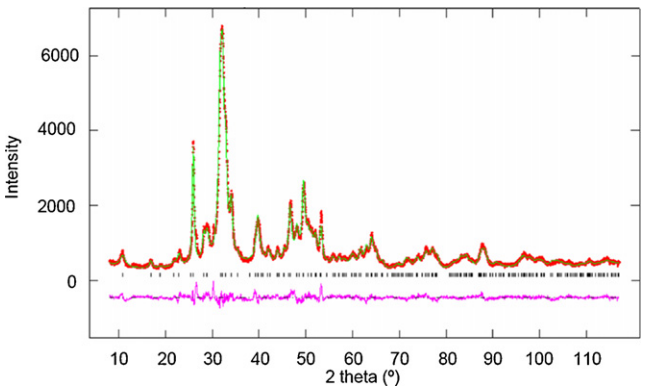

Fig. 7. XRD pattern (+++) and Rietveld refinement fit (—) of a mechanosynthesised CDHA (Ca/P = 1.5)) replicate #1. The tick marks are expected peak positions and the line below is the difference between experimental and calculated profile.

atoms should have been lost in a CDHA to compensate for PO_4^{3-} substitution by HPO_4^{2-}. This high Ca2 occupancy makes the calculated Ca/P molar ratio (1.694 ± 0.11) rather high compared to the Ca/P ratio measured by ICP-OES of 1.56 ± 0.07. Similar differences were found by Wilson et al. [34] in CDHAs obtained by precipitation. The main reason for the high occupancy of Ca II sites could be that the surface hydrated layer of the crystals are expected to be rich in bivalent species (especially HPO_4) and thus the apatite domains, which are the only ones observed by XRD, should contain less HPO_4 than given by the global chemical composition, and consequently the apatite domain should be more "stoichiometric" than expected with a resulting high Ca2 sites occupancy.

Regarding the positional parameters (Table 4) the largest shift expressed as the mean of the five refinements minus mean high temperature HA [19] is in z for O(H) (−0.019), which shows that the OH^- ion has moved 0.140 Å from its HA position away from the mirror plane at $z = 1/4$. Wilson et al. [34] found a 0.103 Å displacement. Both of these displacements are much larger than the ones found in other substituted HAs (0.079 Å in dental enamel [28] or 0.048 Å in a precipitated carbonate apatite [29]). The shifts for all the atoms can be seen in last row of Table 4. The most important shifts apart from O(H)z are O1x (0.012), O2x (0.012), O1y (0.0091) and Ca2x (0.0084).

4. Conclusions

It is possible to obtain nanocrystalline calcium deficient HAs (CDHAs) by dry mechanosynthesis from dicalcium phosphate dihydrate (DCPD) and calcium oxide (CaO) with an analogous structure to nanocrystalline CDHAs obtained by aqueous methods. Lattice parameters of mechanosynthesised CDHA with Ca/P molar ratio of 1.5 showed a small increase in the ***a*** lattice parameter (9.4418(20) Å) and a small decrease in the ***c*** lattice parameter (6.8745(17) Å), in agreement with the values reported in the literature for precipitated CDHAs. Moreover, spectroscopic techniques have shown the existence of HPO_4^{2-} groups in both the ususal apatitic environment and a non-apatitic environment, which has been attributed to the existence of anhydrated surface layer due to the nano-dimensions of the apatitic crystals. Recent studies point out that this layer would play a key role in biomineralization processes. Dry mechanosynthesis has been already proved to be an efficient technique to introduce several ionic substitutions in the apatite lattice. Thus, dry mechanosynthesis produces nanocrystalline CDHAs that can be of interest for several biotechnology applications.

Acknowledgements

The authors would like to acknowledge Prof. P. Boudeville for his help in the synthesis of the calcium deficient hydroxyapatite by means of dry mechanosynthesis, as well as Prof. J.C. Elliott for the fruitful discussions about the mechanosynthesised calcium deficient hydroxyapatite structure. The authors also thank the Spanish Ministry of Education and Science for funding this work through project MAT2009-13547 and Dr. Montserrat Espanol and Dr. Cristina Canal for her technical assistance. Support for the research of M.P. Ginebra was received through the prize ICREA Academia for excellence in research, funded by the Generalitat de Catalunya.

References

[1] F.C.M. Driessens, R.M.H. Verbeeck, Biominerals, Boca Raton, Florida, 1990.
[2] R.Z. LeGeros, Calcium Phosphates in Oral Biology and Medicine, Karger, Basel, 1991.
[3] C. Drouet, F. Bosc, M. Banu, C. Largeot, C. Combes, G. Dechambre, C. Estournes, G. Raimbeaux, C. Rey, Powder Technol. 190 (2009) 118–122.
[4] H.K. Schmidt, Mol. Cryst. Liquid Cryst. 353 (2000) 165–179.
[5] Y.R. Cai, Y.K. Liu, W.Q. Yan, Q.H. Hu, J.H. Tao, M. Zhang, Z.L. Shi, R.K. Tang, J. Mater. Chem. 17 (2007) 3780–3787.
[6] Q.H. Hu, Z. Tan, Y.K. Liu, J.H. Tao, Y.R. Cai, M. Zhang, H.H. Pan, X.R. Xu, R.K. Tang, J. Mater. Chem. 17 (2007) 4690–4698.
[7] S.V. Dorozhkin, Acta Biomater. 6 (2010) 715–734.
[8] M. Wei, A.J. Ruys, B.K. Milthorpe, C.C. Sorrell, J. Mater. Sci.: Mater. Med. 16 (2005) 319–324.
[9] I. Mobasherpour, M.S. Heshajin, A. Kazemzadeh, M. Zakeri, J. Alloy. Compd. 430 (2007) 330–333.
[10] G.W.C. Silva, L.Z. Ma, O. Hemmers, D. Lindle, Micron 39 (2008) 269–274.
[11] T.A. Kuriakose, S.N. Kalkura, M. Palanichamy, D. Arivuoli, K. Dierks, G. Bocelli, C. Betzel, J. Cryst. Growth 263 (2004) 517–523.
[12] M. Espanol, J. Portillo, J.M. Manero, M.P. Ginebra, Cryst. Eng. Comm. 12 (2010) 3318–3326.
[13] M.P. Ginebra, F.C.M. Driessens, J.A. Planell, Biomaterials 25 (2004) 3453–3462.
[14] E.G. Avvakumov, M. Senna, N. Kosova, Soft Mechanochemical Synthesis a Basis for New Chemical Technologies, Kluwer Academic Publishers, Boston, 2001.
[15] K.C.B. Yeong, J. Wang, S.C. Ng, Biomaterials 22 (2001) 2705–2712.
[16] P. Boudeville, B. Pauvert, M.P. Ginebra, E. Fernandez, J.A. Planell, Key Eng. Mater. 192–1 (2000) 115–118.
[17] C. Mochales, H. El Briak-BenAbdeslam, M.P. Ginebra, A. Terol, J.A. Planell, P. Boudeville, Biomaterials 25 (2004) 1151–1158.
[18] H. El Briak-BenAbdeslam, C. Mochales, M.P. Ginebra, J. Nurit, J.A. Planell, P. Boudeville, J. Biomed. Mater. Res. 67A (2003) 927–937.
[19] S. Serraj, P. Boudeville, B. Pauvert, A. Terol, J. Biomed. Mater. Res. 55 (2001) 566–575.
[20] C. Mochales, H. El Briak-BenAbdeslam, M.P. Ginebra, P. Boudeville, J.A. Planell, Key Eng. Mater. 254–2 (2004) 107–110.
[21] J.F. Liao, K. Hamada, M. Senna, J. Mater. Synth. Process. 8 (2000) 305–311.
[22] M.H. Fathi, E.M. Zahrani, J. Cryst. Growth 311 (2009) 1392–1403.
[23] W.L. Suchanek, K. Byrappa, P. Shuk, R.E. Riman, V.F. Janas, K.S. TenHuisen, Biomaterials 25 (2004) 4647–4657.
[24] W.L. Suchanek, P. Shuk, K. Byrappa, R.E. Riman, K.S. TenHuisen, V.F. Janas, Biomaterials 23 (2002) 699–710.
[25] J. Ballon, V. Comparat, J. Pouxe, Nucl. Instrum. Methods Phys. Res. 217 (1983) 213–216.
[26] M. Evain, P. Deniard, A. Jouanneaux, R. Brec, J. Appl. Cryst. 26 (1993) 563–569.
[27] K. Sudarsanan, R.A. Young, Acta Cryst. B 25 (1969) 1534–1543.
[28] R.M. Wilson, J.C. Elliott, S.E.P. Dowker, Am. Miner. 84 (1999) 1406–1414.
[29] H. Morgan, R.M. Wilson, J.C. Elliott, S.E.P. Dowker, P. Anderson, Biomaterials 21 (2000) 617–627.
[30] J.C. Elliott, Hydroxyapatite, Nonstoichiometric apatites, in: Structure and Chemistry of the Apatites and Other Calcium Orthophosphates, Elsevier, Amsterdam, 1994, pp. 111-189.
[31] C. Rey, C. Combes, C. Drouet, A. Lebugle, H. Sfihi, A. Barroug, Werkstofftech 38 (2007) 996–1002.
[32] C. Rey, C. Combes, C. Drouet, H. Sfihi, A. Barroug, Mater. Sci. Eng. C: Biomimetic Supramol. Syst. 27 (2007) 198–205.
[33] W.P. Rothwell, J.S. Waugh, J.P. Yesinowski, J. Am. Chem. Soc. 102 (1980) 2637–2643.
[34] R.M. Wilson, J.C. Elliott, S.E.P. Dowker, L.M. Rodriguez-Lorenzo, Biomaterials 26 (2005) 1317–1327.
[35] A. Kaflak-Hachulska, A. Samoson, W. Kolodziejski, Calcif. Tissue Int. 73 (2003) 476–486.
[36] L.M. Rodriguez-Lorenzo, J. Mater. Sci.: Mater. Med. 16 (2005) 393–398.
[37] J.P. Yesinowski, H. Eckert, J. Am. Chem. Soc. 21 (1987) 6274–6282.
[38] C. Jager, T. Welzel, W. Meyer-Zaika, M. Epple, Magn. Reson. Chem. 44 (2006) 573–580.